

# MMGAN: Generative Adversarial Networks for Multi-Modal Distributions

**Teodora Pandeva and Matthias Schubert**

Institute for Informatics

LMU Munich

Teodora.Pandeva@campus.lmu.de and schubert@dbs.ifi.lmu.de

## Abstract

Over the past years, Generative Adversarial Networks (GANs) have shown a remarkable generation performance especially in image synthesis. Unfortunately, they are also known for having an unstable training process and might lose parts of the data distribution for heterogeneous input data. In this paper, we propose a novel GAN extension for multi-modal distribution learning (MMGAN). In our approach, we model the latent space as a Gaussian mixture model with a number of clusters referring to the number of disconnected data manifolds in the observation space, and include a clustering network, which relates each data manifold to one Gaussian cluster. Thus, the training gets more stable. Moreover, MMGAN allows for clustering real data according to the learned data manifold in the latent space. By a series of benchmark experiments, we illustrate that MMGAN outperforms competitive state-of-the-art models in terms of clustering performance.

## Introduction

Generative Adversarial Nets (GANs) (Goodfellow et al. 2014) are state-of-the-art deep generative models and, therefore, they are primarily designed to model data distributions. Compared to other generative models, GANs gain distinction in generating higher quality data. Despite their notable success, GANs still suffer from unsolved problems and thus, there is ongoing research to further improve their performance and make training more stable. For instance, GAN implicit nature does not allow to apply inference learning on the latent space. Although many methods exist which deal with this shortcoming most of them lack interpretability of the estimated posterior distribution. Moreover, GANs model the latent space as a simple unimodal distributions, ignoring the often more complicated implicit structure of the learned data distribution. However, for many data sets, a union of disjoint manifolds (or clusters) fits more naturally to the implicit structure of the input data. For example, digit data can be interpreted as samples from a disjoint union of 10 manifolds – one for each digit. (Khayatkhoei, Singh, and Elgammal 2018) showed that the quality of generated data suffers from the generator attempting to cover all data manifolds in the data space with a single manifold in the latent space.

Hence, this can lead to mode dropping, i.e. one or more sub-manifolds of the real data are not covered by the generator. It has been proven that GAN’s local convergence can be sustained when the real and fake data distribution are near achieving a Nash equilibrium (Nagarajan and Kolter 2017). Thus, ignoring the multi-modal nature of a data set might lead to oscillating generator parameters without converging to the real distribution.

In this paper, we introduce GANs for learning multi-modal distributions. The resulting architecture, which is named MMGAN, adopts a dynamic disconnected structure of the latent space, which is distributed according to a Gaussian mixture model. More precisely, by introducing an extra network into the GAN structure, the resulting framework aims to find a disconnected data representation in the latent space, such that each data mode or cluster in the observation space is related to a single cluster in the latent space. This stabilizes the training process and yields a better data representation. Furthermore, we can do inference on the real data to predict the most likely cluster in the latent space and thus, categorize the data with respect to its implicit structure. We provide an universal approximation theorem assuring the existence of a generator with the MMGAN functionality in the spirit of (Cybenko 1989; Hornik 1991).

## Related Work

There is a great variety of GAN architectures, which explore the latent space abilities to produce realistic data. Most of them can be referred to as hybrid VAE-GAN methods, which bridge the gap between Variational Autoencoders (VAEs) (Kingma and Welling 2013) and GANs. All of them use a third encoder network which maps a data object to an instance from the latent space  $\mathcal{Z}$ . For example, Makhzani et al. proposed the Adversarial Autoencoder (AAE), which is an autoencoder for performing inference. AAE is composed of three networks: encoder, decoder and discriminator. The latter is trained to correctly classify an encoded noise from the prior noise, which is an arbitrary noise distribution. Although this model can be extended to learn a discrete data representation in an unsupervised learning fashion, it does not consider the true data distribution. Another VAE-GAN

hybrid is ClusterGAN (Mukherjee et al. 2018), which is essentially InfoGAN (Chen et al. 2016) followed by k-means post-clustering on the encoded latent codes. Although InfoGAN has shown remarkable generation and clustering performance by semantically disentangling the latent space, we argue that the encodings are not suitable for  $k$ -means clustering, which tends to discover spherical patterns in the data.

A further approach for gaining more insights into the structure of the noise  $\mathcal{Z}$ , is to directly model the latent space by imposing some assumptions about the prior distribution  $\mathbb{P}_z$ . For instance, GM-GAN (Ben-Yosef and Weinsall 2018) and DeLiGAN (Gurumurthy, Sarvadevabhatla, and Babu 2017) adopt a Gaussian mixture model for the latent space distribution, where the means and standard deviations are learnable parameters. However, these models do not provide any direct inference framework and any interpretation of the learned latent components.

The Gaussian Mixture VAE (GMVAE) is adapted for unsupervised clustering tasks as the latent space  $\mathcal{Z}$  attains the form of Gaussian mixture model (Dilokthanakul et al. 2016). Thus, it becomes the explicit counterpart of MMGAN. However, based on the VAE framework, GMVAE has shown some shortcomings, including the VAE’s tendency to produce blurry images and the (strong) restriction of the encoder output distribution.

## Generative Adversarial Networks

GANs consist of two networks which are opposed to one another in a game (Goodfellow et al. 2014). The first one,  $G$ , is a **generator**, which captures the data distribution and tries to produce realistic data. It receives as input noise data, sampled from the latent space  $\mathcal{Z} \subset \mathbb{R}^d$  with dimension  $d$ , which is deterministically mapped to a data point from the observation space  $\mathcal{X} \subset \mathbb{R}^p$ , where  $p \geq d$ . The second player,  $D$ , is called **discriminator**. It measures how realistic the input data is, i.e. for some  $x \in \mathcal{X}$ ,  $D(x)$  is in general a score, e.g. the probability, measuring whether  $x$  comes from the real distribution. Thus,  $D$  is trained via supervised learning on data with assigned labels 1 for being real and 0 for being fake and tries to correctly classify a real object from a fake one. In contrast,  $G$  aims to fool the discriminator by producing data resembling the real data as close as possible.

In this setting, the models  $D$  and  $G$  are neural networks with fixed structures. Hence, the learning takes place over the networks parameters, which are denoted by  $\theta_D \in \Theta_D$  and  $\theta_G \in \Theta_G$ , respectively, where  $\Theta_D$  and  $\Theta_G$  are real spaces with dimension depending on the networks architectures. For simplicity, throughout this work, we use  $G(z)$  and  $D(x)$  instead of  $G(z; \theta_G)$  and  $D(x; \theta_D)$ , respectively, unless it is explicitly mentioned. Here, the unknown true data distribution is denoted by  $\mathbb{P}_r$ , defined on  $\mathcal{X}$ , and  $\mathbb{P}_z$  is the input noise distribution, defined on  $\mathcal{Z}$ . Given a noise instance  $z$ , the generator produces a fake data point  $x_f = G(z)$ , which is a sample of the unspecified distribution, induced by  $\mathbb{P}_f$ , which is the implicit approximation of  $\mathbb{P}_r$  and gives the methodology how  $\mathcal{Z}$  is related to  $\mathcal{X}$ .

The standard GAN optimization problem (SGAN) (Good-

fellow et al. 2014) is defined by

$$\hat{\theta}_D, \hat{\theta}_G = \arg \min_{\theta_D} \arg \max_{\theta_G} V(D, G) \text{ with}$$

$$V(D, G) = -\mathbb{E}_{x_r \sim \mathbb{P}_r} [\log(D(x_r))] - \mathbb{E}_{x_f \sim \mathbb{P}_f} [\log(1 - D(x_f))].$$

Jolicoeur-Martineau gives a theoretical and empirical analysis of the SGAN training behavior which contradicts the theoretical results, derived by (Goodfellow et al. 2014), i.e. the probability of real data being real should decrease during training, while the probability of fake data being fake should increase, which is not fulfilled by SGAN. To excel the training stability, *relativistic* objective functions are proposed (Jolicoeur-Martineau 2018). A class representative is the RSGAN, defined in the initial paper. The corresponding optimization problem is given by

$$\hat{\theta}_D = \arg \min_{\theta_D} -\mathbb{E}_{x_r \sim \mathbb{P}_r, x_f \sim \mathbb{P}_f} [\log(s(C(x_r)) - C(x_f))] \\ \hat{\theta}_G = \arg \min_{\theta_G} -\mathbb{E}_{x_r \sim \mathbb{P}_r, x_f \sim \mathbb{P}_f} [\log(s(C(x_f)) - C(x_r))],$$

where  $C(\cdot)$  is the critic of the discriminator, which is defined by the non-transformed output of  $D$  (Arjovsky, Chintala, and Bottou 2017), i.e.  $C(x) = \text{logit}(D(x))$ , and  $s : \mathbb{R} \cup \{-\infty, +\infty\} \rightarrow [0, 1]$ ,  $s(x) = (1 + \exp(-x))^{-1}$  is the sigmoid function. This is equivalent to the negative expected probability that a real data object is more realistic than a fake one. A further example of the relativistic approach is the relativistic average GAN (RaSGAN), which compares a real object to the average fake one and vice versa. We provide a modified version of RaSGAN in the next section. Notably, this family of objective functions allows a direct comparison between pairs of fake and real data objects. This is a key feature which is utilized in the MMGAN structure.

## Multi-Modal GANs (MMGAN)

MMGAN samples noise from a Gaussian mixture model. In particular, we sample a cluster from a cluster distribution  $\text{Cat}\left(K, \frac{1}{K}\right)$  and then, draw the noise  $z$  from the Gaussian corresponding to the sampled cluster. As any GAN, MMGAN takes  $z$  as input to a generator ( $G$ ) and employs a discriminator ( $D$ ) to guide  $G$  to generate realistic objects. In addition, MMGAN employs an encoder network ( $E$ ) to predict the cluster of data objects. The output is a probability distribution over the clusters, which is denoted by  $p_E(\cdot|x)$  for  $x \in \mathcal{X}$ . Thus, the encoder  $E$  should reproduce the cluster from which a fake instance was sampled from, and predict the most likely cluster for real images. An overview of the architecture is depicted in Figure 1.

In the following, we will describe our architecture in more detail. To force MMGAN to cluster data, we model the latent space as a mixture of Gaussians with a uniform prior over the clusters. Thus, our goal is to find a representation of each cluster in terms of mean and covariance. We restrict the covariance matrix to have equal diagonal entries and 0 everywhere else, i.e. to be of the form  $\sigma^2 \mathbb{I}_d$  where  $\sigma \in \mathbb{R}$ . Therefore, we define the pairing  $(\mu_k, \sigma_k)$  with  $\mu_k \in \mathbb{R}^d$  and

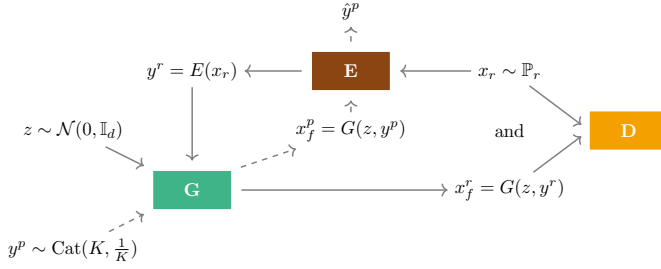


Figure 1: MMGAN architecture consists of three networks: generator, discriminator and encoder. There are two training cycles. The solid lines show the data flow for building pairs between a real and a fake sample. The discriminator  $D$  is trained on the formed pairings (batch  $B1$ ). The dashed lines follow the generation of prior data from a randomly sampled cluster (batch  $B2$ ). Thus, the encoder  $E$  learns to correctly classify an  $x_f^p$  with a true label  $y^p$ .

$\sigma_k \in \mathbb{R}$  to be the mean and standard deviation of the  $k$ th cluster, where for all  $k \in \{0, \dots, K\}$ ,  $(\mu_k, \sigma_k)$  are learnable parameters. Both parameters are represented by a  $K \times d$  and  $K \times 1$  dense layers located right before the core generator, denoted by  $\mu$  and  $\sigma$ , respectively. Both networks receive a one hot encoded cluster as input, i.e. of the form  $y = (0, \dots, 1, \dots, 0)$ , and output  $\mu_k := \mu(y)$  and  $\sigma_k := \sigma(y)$  for the  $k^{\text{th}}$  entry of  $y$  being 1, i.e.  $y_k = 1$ . Thus, for the cluster related noise  $\tilde{z}$ , we obtain  $\tilde{z} = \mu(y) + \sigma(y)z$  using the reparameterization trick (Kingma and Welling 2013). Afterwards  $\tilde{z}$  is fed into the core generator. The exact procedure is illustrated in Figure 2. To formalize the whole procedure, we describe the generative model  $\mathbb{P}_f$  as:

$$y \sim \text{Cat}\left(K, \frac{1}{K}\right),$$

$$\tilde{z}|y \sim \mathcal{N}(\mu(y), \sigma(y)^2 \mathbb{I}_d),$$

$$x_f = G(\tilde{z}),$$

Doing inference on the latent space can be done by directly computing the posterior  $p(z|x)$  for  $z \in \mathcal{Z}$  and  $x \in \mathcal{X}$ , i.e.

$$p(z|x) = \sum_{k=1}^K p_E(y|x) \mathcal{N}(z|\mu_k, \sigma_k^2 \mathbb{I}_d),$$

where  $\mathcal{N}(z|\mu_k, \sigma_k^2 \mathbb{I}_d)$  denotes the probability distribution function of  $\mathcal{N}(\mu_k, \sigma_k^2 \mathbb{I}_d)$ .

## MMGAN Training

To explain the training of MMGANs, we will start with the generation of training batches. Firstly, we sample real objects  $x_r$  from the unknown distribution  $\mathbb{P}_r$ . These are fed into the encoder  $E$ , such that the resulting output is transformed into a cluster  $y^r$ , which refers to a Gaussian cluster in the mixture model. The encoded  $y^r$  together with randomly sampled standard Gaussian noise serve as an input to the generator  $G$ . Thus, fake objects  $x_f^r$  are produced from the Gaussian cluster, corresponding to the sampled real data

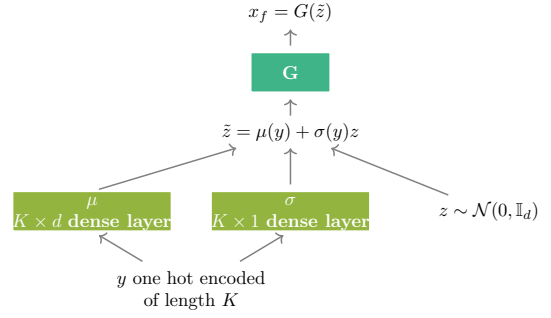


Figure 2: The generator is extended by two layers representing the cluster mean and standard deviation. Their input is the cluster which is one hot encoded. Hence, the noise  $z$  is transformed into a Gaussian variable with mean  $\mu(y)$  and  $\sigma(y)^2 \mathbb{I}_d$  variance.

$x_r$ . The resulting pairings  $(x_r, x_f)$  are fed into the discriminator  $D$ . We argue that this pairing system will excel both the data generation process and the clustering performance. We will refer to this training batch as **B1**.

In addition, to train the encoder  $E$  to correctly assign clusters to fake objects, we generate a second type of training batch, **B2**, which is composed of fake observations  $x_f^p$  labeled by their corresponding clusters  $y^p$ . For this batch, the clusters  $y^p$  are randomly drawn samples from the categorical distribution  $\text{Cat}(K, \frac{1}{K})$ .

The exact optimization problem for training MMGANs is given as follows:

$$\min_{\theta_D} \max_{\theta_G, \theta_E} V(D, G, E) + \alpha \mathbb{E}_{y \sim \text{Cat}(K, \frac{1}{K}), z \sim \mathcal{N}(0, \mathbb{I}_d), x_f = G(z, y)} [\log p_E(y|x_f)],$$

where  $V(D, G, E)$  refers to an adversarial loss, depending on the three nets, and  $p_E(\cdot|x)$  is the output encoder posterior for given observation  $x \in \mathcal{X}$ . Note that  $V(D, G, E)$  is trained on the first type of batch **B1** and thus, depends on  $E$  to generate fake instances  $x_f$ . The second term is the cross entropy loss for the encoder output, weighted by a hyperparameter  $\alpha > 0$ . This term is trained on the second type of batch **B2** to make sure that each cluster is sufficiently represented.

The training steps are shown in Algorithm 1. To lay emphasis on the dependence of  $V(D, G, E)$  on the parameters  $\theta_D, \theta_G$  and  $\theta_E$ , in Algorithm 1, the notation  $D(\cdot; \theta_D)$ ,  $G(\cdot; \theta_G)$  and  $E(\cdot; \theta_E)$  is used. Here, the chosen adversarial loss is RSGAN. Moreover, we use Adam (Kingma and Ba 2015) for parameter learning (see lines 12–13 of Algorithm 1).

We choose  $V(D, G, E)$  to be a relativistic objective since we aim to measure similarity between real and fake objects, belonging to the same cluster. If we assume that  $E$  clusters data objects in a meaningful way, we expect that the discriminator will find it more difficult to classify a real object  $x_r$  from a fake one  $x_f$  from the same mode. Thus, we argue that the discriminator will not reach optimality very fast, which

---

**Algorithm 1** MMGAN

---

**1: Input:**

$K$ : number of clusters  
 $train\_iter$ : number of training iterations  
 $m$ : batch size  
 $d$ : noise dimension  
 $\alpha$ : hyperparameter

2: Initialize  $\theta_D^0, \theta_G^0, \theta_E^0$ .3: **for**  $t = 1$  to  $train\_iter$  **do**4:   Sample  $x_r$  from data of size  $m$ .5:    $y = E(x_r; \theta_E^{t-1})$ 6:   Sample  $y^p \sim \text{Cat}(K, \frac{1}{K})$  of size  $m$ .7:   Sample  $z \sim \mathcal{N}(0, \mathbb{I}_d)$  of size  $m$ .8:    $x_f = G(z, y; \theta_G^{t-1})$ 9:    $x_f^p = G(z, y^p; \theta_G^{t-1})$ 10:    $l_D^{t-1} = -\frac{1}{m} \left( \sum_{i=1}^m \nabla_{\theta_D} \log(s(C(x_r^{(i)}; \theta_D^{t-1}) - C(x_f^{(i)}; \theta_D^{t-1}))) \right)$ 11:    $l_{G,E}^{t-1} = -\frac{1}{m} \left( \sum_{i=1}^m \nabla_{(\theta_G, \theta_E)} \log(s(C(x_f^{(i)}) - C(x_r^{(i)}))) + \alpha \log p_E(y^p(i) | x_f^p(i)) \right)$ 12:   Update  $\theta_D^{t-1}$  by Adam with gradient  $l_D^{t-1}$ .13:   Update  $(\theta_G^{t-1}, \theta_E^{t-1})$  by Adam with gradient  $l_{G,E}^{t-1}$ .**14: Output:** $D, G, E$ 

---

will lead to a more stable GAN training behavior (Arjovsky and Bottou 2017).

In addition to using standard RSGAN loss, we propose an extension of the RaSGAN (Jolicœur-Martineau 2018), which is a cluster-wise comparison between a real data object and the average fake one or vice versa, i.e.  $\hat{\theta}_D, \hat{\theta}_G$  and  $\hat{\theta}_E$  are optimal solutions of the optimization problems

$$\hat{\theta}_D = \min_{\theta_D} - \mathbb{E}_{x_r \sim \mathbb{P}_r} [\log \hat{D}(x_r)] - \mathbb{E}_{z \sim \mathbb{P}_z, y \sim \text{Cat}(K, \frac{1}{K})} [\log(1 - \hat{D}(G(z, y)))],$$

$$\hat{\theta}_G, \hat{\theta}_E = \min_{\theta_G, \theta_E} - \mathbb{E}_{z \sim \mathbb{P}_z, y \sim \text{Cat}(K, \frac{1}{K})} [\log \hat{D}(G(z, y))] - \mathbb{E}_{x_r \sim \mathbb{P}_r} [\log(1 - \hat{D}(x_r))],$$

where

$$\hat{D}(x_r) = s(C(x_r) - \mathbb{E}_{z \sim \mathbb{P}_z} [C(G(z, E(x_r)))])$$

$$\hat{D}(G(z, y)) = s(C(G(z, y)) - \mathbb{E}_{x_r \sim \mathbb{P}_r} [\delta_{E(x_r)}(y) \cdot C(x_r)]),$$

and  $\delta_{E(x_r)}(y)$  is the Dirac delta function with  $\delta_{E(x_r)}(y) = 1$  for  $E$  assigning the highest probability of  $x_r$  being in cluster  $y$ , and 0 otherwise. We name the resulting objective conditional RaSGAN (cRaSGAN).

**Universal Approximation Theorem for the Latent Space Assumption**

In the following, we will guarantee the existence of a fully connected neural network that maps a collection of Gaus-

sians to the disjoint data space such that the resulting network recovers the initial data distribution up to a constant  $\epsilon$ . This result is closely related to the Universal Approximation Theorem of (Cybenko 1989; Hornik 1991). A similar theory for the uniform distribution has been recently developed in the work of (Khrulkov and Oseledets 2019).

Here, we are interested in *smooth* (infinitely differentiable) functions  $f$ , which surjectively map the support of a Gaussian distribution to a  $d$ -connected manifold, as defined in (Jost, Jürgen 2008, Definition 1.4.1). In real life applications, we choose the dimensionality of the latent space  $\mathcal{Z} \subseteq \mathbb{R}^d$  to be very large, due to the high dimensionality of the observation space  $\mathcal{X}$ . The Gaussian Annulus theorem (see (Blum, Hopcroft, and Kannan 2015, Theorem 2.9)) suggests that for a large enough  $d$ , the mass of a Gaussian with zero mean and identity matrix as covariance is concentrated around the periphery of a ball with radius  $\sqrt{d-1}$  and, thus, it approximates the sphere  $\sqrt{d-1} \cdot \mathbb{S}^{d-1} = \{x \in \mathbb{R}^d \mid \|x\|_2^2 = d-1\}$ . The theory developed below is adapted to high dimensional spherical latent spaces, since these can be easily extended to high dimensional Gaussians.

**Lemma 1.** *Let  $\mathcal{M} \subset \mathbb{R}^p$  for  $p \geq d$  be a compact connected  $d$ -dimensional manifold. Then there exists a smooth map*

$$f : \mathbb{S}^d \rightarrow \mathbb{R}^p,$$

such that  $f(\mathbb{S}^d) = \mathcal{M}$ , where  $\mathbb{S}^d = \{x \in \mathbb{R}^{d+1} \mid \|x\|_2 = 1\}$ .

*Proof.* We use (Khrulkov and Oseledets 2019, Theorem 5.1), implying the existence of a surjective smooth map  $g : \overline{\mathcal{B}_d^1(0)} \rightarrow \mathcal{M}$ , where  $\overline{\mathcal{B}_d^1(0)}$  is the (closed  $d$ -dimensional) unit ball with origin 0, i.e.  $\overline{\mathcal{B}_d^1(0)} = \{x \in \mathbb{R}^d \mid \|x\|_2 \leq 1\}$ . Now, we construct a smooth surjective function  $\phi : \mathbb{S}^d \rightarrow \overline{\mathcal{B}_d^1(0)}$ , such that the resulting map  $f := g \circ \phi$ , i.e.  $f(x) = g(\phi(x))$  for all  $x \in \mathbb{S}^d$ , fulfills the above stated requirements.

Let  $\phi : \mathbb{S}^d \rightarrow \overline{\mathcal{B}_d^1(0)}$  be the projection on the unit ball defined by  $\phi(x) = (x_1, \dots, x_d)^T$  for  $x \in \mathbb{S}^d$ . This map is smooth because it can be represented in matrix form by  $A = \text{diag}(\underbrace{1, \dots, 1}_{d \text{ times}}, 0)$ , such that  $\phi(x) = Ax$ . It is also surjective

because for each  $y \in \overline{\mathcal{B}_d^1(0)}$  the point  $x = (y_1, \dots, y_p, (1 - \sum_{i=1}^p y_i^2)^{1/2})$  fulfills  $\phi(x) = y$  and is contained in  $\mathbb{S}^d$  since  $\|x\|_2 = 1$ .

Thus, the map  $f := \phi \circ g$  is smooth and surjective since it is a composition of smooth and surjective maps.  $\square$

Let  $\mathcal{Z}$  be the support of a  $d+1$ -dimensional Gaussian of the form  $\mathcal{N}(0, \mathbb{I}_{d+1})$ . Hence, the map  $g : \mathcal{Z} \rightarrow \mathcal{M}$ ,  $g(x) = f\left(\frac{x}{\|x\|_2}\right)$ , where  $f$  is defined as in Lemma 1, is smooth and  $g(\mathcal{Z}) = \mathcal{M}$ , since  $\frac{x}{\|x\|_2} \in \mathbb{S}^d$ .

According to the Universal Approximation Theorem by (Cybenko 1989; Hornik 1991) the map defined in Lemma 1 can be approximated by a fully-connected neural network arbitrarily well. This observation is translated into the more general case of disconnected manifolds in Theorem 1. In this setting, the approximation error is measured by means of

the Hausdorff distance  $d_H$  (Munkres 2017, p. 280), which is defined by

$$d_H(X, Y) = \max\left\{\sup_{x \in X} \inf_{y \in Y} m(x, y), \sup_{y \in Y} \inf_{x \in X} m(x, y)\right\},$$

where  $m$  is a well-defined metric on  $\mathbb{R}^d$  and  $X, Y \subseteq \mathbb{R}^d$ . Thus, we aim to find a network  $G$  such that the value for  $d_H(G(\mathcal{Z}), \mathcal{X})$  is kept to be low.

**Theorem 1.** *Let  $\mathcal{X} = \bigcup_{i=1}^K \mathcal{X}_i \subset \mathbb{R}^p$ ,  $p \geq d$  be a disconnected union of compact connected  $d$ -dimensional manifolds. Then for every  $\epsilon > 0$  and every nonconstant, bounded, continuous activation function  $\phi : \mathbb{R} \rightarrow \mathbb{R}$ , there exists a fully connected neural network  $G : \mathbb{R}^{d+1} \rightarrow \mathbb{R}^p$  with activation function  $\phi$  such that the following is fulfilled.*

*There exists a collection  $\{S_i\}_{i=1}^K$  of disjoint  $d + 1$ -dimensional compact annuli such that for all  $i \in \{1, \dots, K\}$*

$$d_H(G(S_i), \mathcal{X}_i) < \epsilon.$$

*Proof.* The collection  $\{S_i\}_{i=1}^K$  is constructed explicitly. Let  $D = [-2\sqrt{d}, 2\sqrt{d}]^{d+1}$  be a  $d + 1$ -dimensional cube and  $\{v_1, \dots, v_{2^{d+1}}\}$  be the set of all vertices, i.e. for all  $i \in \{1, \dots, 2^{d+1}\}$ ,  $v_i \in [-2\sqrt{d}, 2\sqrt{d}]^{d+1}$ . We choose arbitrarily  $K$  vertices  $\{v_{(1)}, \dots, v_{(K)}\} \subseteq \{v_1, \dots, v_{2^{d+1}}\}$  and initialize  $K$  Gaussians with mean  $v_{(i)}$  and covariance  $\mathbb{I}_{d+1}$  for  $i \in \{1, \dots, K\}$ . Now, by means of the Gaussian Annulus Theorem (defined as in (Hopcroft and Kannan 2013, Lemma 2.4)), the required sets  $S_i$  are defined as annuli, i.e.  $S_i = \{x \in \mathbb{R}^{d+1} | \sqrt{d} - \delta \leq \|x - v_{(i)}\|_2 \leq \sqrt{d} + \delta\}$ , for some  $0 < \delta < \sqrt{d}$ , where every  $S_i$  contains the support of the  $i$ -th Gaussian up to a fraction of  $\frac{4}{\delta^2} e^{-\delta^2/4}$ . Thus the initialized annuli form a union of disjoint compact  $d + 1$ -connected manifolds.

Lemma 1 conveys that for every given manifold  $\mathcal{X}_i$ , there exist a smooth surjective function  $f_i$ , such that  $f_i(S_i) = \mathcal{X}_i$ . Thus, we obtain a collection of functions  $\{f_i\}_{i=1}^K$ . Let  $f : \mathbb{R}^{d+1} \rightarrow \mathbb{R}^d$  be of the form  $f(x) = \sum_{i=1}^K f_i(x) \mathbb{1}_{S_i}(x)$ , where  $\mathbb{1}_{S_i}(x)$  is the indicator function defined on  $S_i$ , i.e.  $\mathbb{1}_{S_i}(x) = 1$  for  $x \in S_i$  and 0 otherwise. Next, we construct a function  $f_\rho$  which is an approximation of  $f$  via smoothing by convolution with a suitable function, e.g. the standard mollifier, defined by:

$$\eta_\rho : \mathbb{R}^{d+1} \rightarrow \mathbb{R},$$

$$\eta_\rho(x) = \begin{cases} \frac{\alpha}{\rho^p} \exp\left(-\frac{\rho^2}{\rho^2 - \|x\|_2^2}\right) & x \in \mathcal{B}_{d+1}^\rho(0), \\ 0 & \text{otherwise} \end{cases},$$

where  $\rho > 0$  and  $\alpha$  is chosen, such that

$$\int_{\mathbb{R}^{d+1}} \eta_\rho(x) dx = 1,$$

and  $\mathcal{B}_{d+1}^\rho(0) = \{x \in \mathbb{R}^{d+1} | \|x\|_2 < \rho\}$ .

Let  $\Omega = \bigcup_i^K S_i \setminus \partial S_i$ , where  $\partial S_i = \{x \in \mathbb{R}^{d+1} | \|x - v_{(i)}\|_2 \in \{\sqrt{d} - \delta, \sqrt{d} + \delta\}\}$ . Hence,  $\Omega$  is a union of open

bounded sets. Thus, the resulting convolved function  $f_\rho$ , defined by

$$f_\rho(x) = f * \eta_\rho(x) = \int_{\Omega} \eta_\rho(y) f(x - y) dy$$

$$= \sum_{i=1}^K \int_{S_i \setminus \partial S_i} \eta_\rho(y) f_i(x - y) \mathbb{1}_{S_i}(x - y) dy,$$

is continuous (e.g. (Heil 2019, Theorem 9.1.5)) and it holds

$$\text{supp}(f_\rho) \subset \bigcup_{i \leq K} \overline{S_i + \mathcal{B}_{d+1}^\rho(0)} = \bigcup_{i \leq K} \overline{S_i + \mathcal{B}_{d+1}^\rho(0)} =: S,$$

where  $S_i + \mathcal{B}_{d+1}^\rho(0) = \{x \in \mathbb{R}^{d+1} | \exists s \in S_i, \exists b \in \mathcal{B}_{d+1}^\rho(0), x = s + b\}$ . We choose  $\rho < \sqrt{d} - \delta$  such that the compact sets  $\overline{S_i + \mathcal{B}_{d+1}^\rho(0)}$  become separable, in the sense that for all  $i, j \in \{1, \dots, K\}$ ,  $\overline{S_i + \mathcal{B}_{d+1}^\rho(0)} \cap \overline{S_j + \mathcal{B}_{d+1}^\rho(0)} = \emptyset$ . For all  $i \in \{1, \dots, K\}$ ,  $s \in S_i$  and  $b \in \mathcal{B}_{d+1}^\rho(0)$  it holds  $\|s + b - v_{(i)}\|_2 < 2\sqrt{d}$ . Recall that the means  $v_{(i)}, v_{(j)}$  for all  $i, j \in \{1, \dots, K\}$  are the vertices of  $D$  defined above. Moreover,

$$4\sqrt{d} \leq \|v_{(i)} - v_{(j)}\|_2 \leq \|v_{(i)} - v_{(j)} - (s + b) + (s + b)\|_2$$

$$\leq \|v_{(i)} - (s + b)\|_2 + \|v_{(j)} - (s + b)\|_2$$

$$< 2\sqrt{d} + \|v_{(j)} - (s + b)\|_2.$$

It follows that  $\|v_{(j)} - (s + b)\|_2 \geq 2\sqrt{d} > \sqrt{d} + \delta + \rho$  and, therefore,  $s + b \notin S_j + \mathcal{B}_{d+1}^\rho(0)$ .

Now, define a cube  $Z := [-R, R]^{d+1} \subset \mathbb{R}^{d+1}$ , where  $R$  is chosen such that  $S \subseteq Z$ . Thus, the function  $f_\rho : Z \rightarrow \mathbb{R}^d$ ,  $f_\rho(S_i) = \mathcal{X}_i$  for all  $i \in \{1, \dots, K\}$ , fulfills the requirements of (Khruikov and Oseledets 2019, Theorem 5.1). Therefore, for all  $\epsilon > 0$  a neural network  $G$  exists, such that for all  $i \in \{1, \dots, K\}$ ,  $d_H(G(S_i), \mathcal{X}_i) < \epsilon$ .  $\square$

Theorem 1 gives theoretical guarantees for the existence of a generator  $G$  and a disconnected latent space such that  $G$  approximates the real data manifolds with small error. However, this holds only if the dimension of  $\mathcal{X}$  is known, which is impossible to estimate in every real life application. Nevertheless this result and the discussion above provide a profound justification of the latent space choice.

## Cluster Initialization

To generate a collection of disjoint Gaussian clusters in a high-dimensional space for initializing the model, we propose the following heuristic. It is based on the idea of the annuli construction suggested in the proof of Theorem 1. For this reason, consider the  $d$ -dimensional cube  $[-1, 1]^d$ , where the number of vertices equals  $2^d$ . Let  $V = \{v_1, \dots, v_M\}$  with  $M = 2^d$  is the set of all vertices, i.e. for each  $i \leq M$ ,  $v_i \in \{-1, 1\}^d$ . We randomly sample a subset from  $V$  of length  $K$  and initialize the means of the Gaussian clusters. Here, we assume that the number of clusters  $K$  does not exceed  $2^d$ , i.e.  $K \leq 2^d$ . All the standard deviations  $\sigma_k$  are initialized with values of at most 1. Moreover, to avoid narrow Gaussian clusters with very small  $\sigma_k$  for  $k \in \{1, \dots, K\}$ , we set a lower bound of 0.1 for the standard deviations.

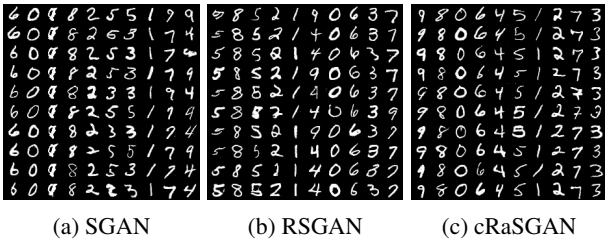


Figure 3: MNIST MMGAN fake images. Each column represents one cluster.

## Experiments

We fix the network structure, parameter initialization and use benchmark data to achieve a fair comparison between our new approach and compared existing models (GMVAE (Dilokthanakul et al. 2016), AAE (Makhzani et al. 2015), ClusterGAN (Mukherjee et al. 2018)). All models are trained with the Adam optimization method (Kingma and Ba 2015), where  $\beta_1 = 0.5$  and  $\beta_2 = 0.99$ . The hyperparameter  $\alpha$  is set to 1 for all experiment. MMGAN and ClusterGAN generator and discriminator use the same architectures as AAE’s decoder and encoder. Moreover, MMGAN/ClusterGAN discriminator and encoder have the same structure. For GMVAE we used an existing implementation<sup>1</sup>. We evaluated our method on a synthetic and three gray scale data sets (Moon (Pedregosa et al. 2011), MNIST (LeCun and Cortes 2010), Fashion MNIST (Xiao, Rasul, and Vollgraf 2017) and Coil-20 (Nene, Nayar, and Murase 1996)). For synthetic data, all model components have two dense layers with 128 units per layer and ReLU activation function while for gray-scale images, MMGAN, ClusterGAN and AAE nets have three CNN layers. The used activation function for the MMGAN/ClusterGAN discriminator and encoder is LeakyReLU.

To study MMGAN functionalities, we conduct several experiments, where the model is trained on benchmarking datasets, and compared to other three competitive models. Table 1 provides an overview of the numerical results regarding the clustering performance on test data. We can conclude that MMGAN especially the cRaSGAN based one outperforms the other competitors in terms of all used evaluation measures: normalized mutual information (NMI), adjusted rank index (ARI), purity (ACC).

Figure 3 illustrates the generated output of SGAN, RSGAN, cRaSGAN - based MMGAN trained on the MNIST data. In this experiment, we can come to the conclusion that the relativistic approach seems to be more stable than the SGAN one. For instance, it can be seen in Figure 3a that the third cluster collapses and clusters 6 and 7 generate the same images. This is illustrated in the 6th and 7th column of Figure 3a.

In Figure 4, the heatmaps visualize cosine similarity between the cluster means, which is defined by  $1 - \cos(\mu_i, \mu_j)$  for two means  $\mu_i$  and  $\mu_j$ , where  $i, j \in \{1, \dots, K\}$ . The measure is bounded in  $[-1, 1]$ . Two clusters are close to each

<sup>1</sup><https://github.com/psanch21/VAE-GMVAE>

Dataset	Model	NMI	ARI	ACC
Moon Data	MMGAN (SGAN)	0.64	0.74	0.93
	MMGAN (RSGAN)	<b>0.76</b>	<b>0.81</b>	<b>0.95</b>
	MMGAN (cRaSGAN)	0.60	0.70	0.92
	GMVAE	0.39	0.47	0.84
	AAE	0.48	0.57	0.86
	ClusterGAN	0.36	0.45	0.83
	MNIST	MMGAN (SGAN)	0.81	0.74
MMGAN (RSGAN)		0.86	0.80	0.88
MMGAN (cRaSGAN)		<b>0.92</b>	<b>0.94</b>	<b>0.97</b>
GMVAE		0.68	0.57	0.70
AAE		0.73	0.64	0.76
ClusterGAN		0.72	0.64	0.74
Fashion MNIST	MMGAN (SGAN)	0.73	0.60	0.74
	MMGAN (RSGAN)	0.67	0.53	0.69
	MMGAN (cRaSGAN)	<b>0.68</b>	<b>0.56</b>	<b>0.70</b>
	GMVAE	0.51	0.32	0.48
	AAE	0.52	0.31	0.50
	ClusterGAN	0.30	0.18	0.42
Coil-20	MMGAN (SGAN)	0.71	0.55	0.67
	MMGAN (RSGAN)	0.76	0.58	0.67
	MMGAN (cRaSGAN)	<b>0.80</b>	<b>0.60</b>	<b>0.72</b>
	GMVAE	0.65	0.29	0.44
	AAE	0.75	0.56	0.61
	ClusterGAN	0.62	0.38	0.45

Table 1: Comparison between MMGAN, GMVAE, AAE and ClusterGAN in terms of the clustering measures NMI, ARI and ACC.

other when the cosine similarity measure is around 1. We also keep in mind that in high dimensional spaces two randomly sampled vectors are almost surely orthogonal. As we have pointed out earlier, clusters 6 and 7 in the SGAN based model generate the same mode. It can be expected that the cluster means form a small angle. However, Figure 4a does not support this hypothesis. The computed cosine measure is around 0. The other two heatmaps (see Figures 4b and 4c) also do not reveal any pattern between the similarity measurements and generated cluster output. For example, the digits 4, 7 and 9 are often associated with one cluster (see column 6 and 10 in 3b). However, according to Figures 4b and 4c the cluster means are not very similar. Herewith, we conclude that the obtained clusters do not allude to further structure in the latent space, i.e. when two latent clusters resemble in  $\mathcal{Z}$ , the corresponding generated output need not be similar in  $\mathcal{X}$ .

In the next experiment, we examine the effect of the pairings strategy on the MMGAN encoder performance. For each dataset (MNIST, Fashion MNIST, Coil-20) five MMGANs are trained using the cRaSGAN adversarial loss. For each dataset, the trained models are evaluated with respect to the clustering measures (NMI, ARI, ACC), which are summarized by their mean and standard deviations, shown in Table 2. Analogously to the setting above, we train MMGANs without using the pairing strategy, i.e. the input noise is sampled randomly from the Gaussian mixture model. Thus, the formed pairings  $(x_r, x_f)$  do not necessarily refer to the same

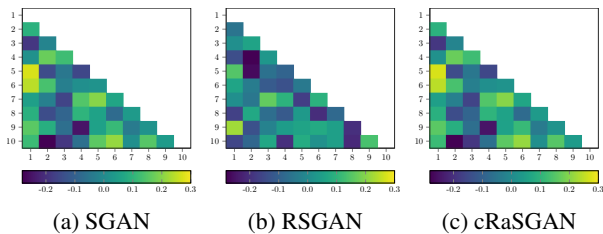


Figure 4: MNIST MMGAN Mean Cosine Similarity. For every model a cosine similarity is computed between the cluster means. The axes represent the clusters and the boxes refer to the pairwise distance between the means, such that high values are indicated by the yellow scale and low values by the blue one.

Dataset	Model	NMI	ARI	ACC
MNIST	MMGAN	<b>0.91 ± 0.03</b>	<b>0.90 ± 0.05</b>	<b>0.94 ± 0.04</b>
	no pairings	0.92 ± 0.01	0.93 ± 0.01	0.96 ± 0.00
Fashion MNIST	MMGAN	<b>0.65 ± 0.01</b>	<b>0.52 ± 0.06</b>	<b>0.66 ± 0.03</b>
	no pairings	0.63 ± 0.01	0.49 ± 0.01	0.63 ± 0.01
Coil-20	MMGAN	<b>0.80 ± 0.01</b>	<b>0.62 ± 0.02</b>	<b>0.73 ± 0.03</b>
	no pairings	0.70 ± 0.02	0.48 ± 0.04	0.64 ± 0.02

Table 2: Comparison between the MMGAN framework and the one without utilizing the pairing strategy in terms of encoder clustering performance.

cluster. Table 2 provides the clustering summary statistics for this type of model, as well.

By considering Table 2, we can conclude that for both the MNIST and Fashion MNIST data the two type of models show similar results in terms of clustering performance. Moreover, in the Coil-20 dataset case, our proposed MMGAN framework outperforms the other one. This observation is also supported by Figure 5, which illustrates the discriminator loss over the training iterations for both type of models. It can be concluded that the random strategy pushes the discriminator loss faster to 0 than the pairings one.

In our experiment, depicted in Figure 6, we trained two MMGANs with different initialization of the cluster means. The first one (see Figure 6a) employs the heuristic explained above, while the second one uses the same starting value for each cluster mean. For both experiments the features standard deviations have starting values 0.5. The latent codes used for acquiring the data points are fixed over all iterations. Interestingly, only after the first iteration a clustered structure can be recognized in the generated data. It can be also seen that the generator manages to reconstruct the initial data distribution and the encoder successfully performs the unsupervised clustering task by achieving maximal evaluation scores. The second row of Figure 6a shows the latent space parameter learning over time. It can be observed that the cluster specific standard deviations decrease. Figure 6b similarly to Figure 6a shows the generator behavior over time, yet for overlapping clustering initialization. It indicates that the resulting encoder does not match the prior labeling. Moreover, the sample quality impairs compared to the first MMGAN.

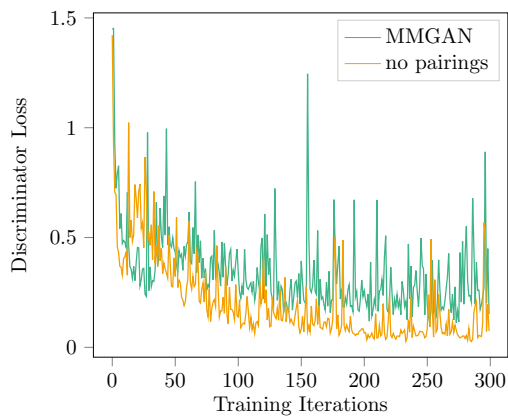


Figure 5: Here, we compare the discriminator loss of the MMGAN model and the one trained without the pairing strategy. Both models are fitted on the Coil-20 dataset.

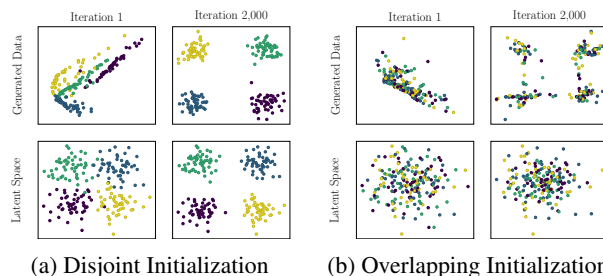


Figure 6: The first row shows a sample of the generated data points over the training iterations, i.e. after the first and 2,000. The second row represents the learned latent space distribution w.r.t the initialization. The coloring refers to the given prior clusters. The model with fixed initialization cannot reconstruct the predefined clusters.

## Conclusions

This paper introduced a new model from the VAE-GANs hybrid family, which is adapted for both inference learning and approximating real data distributions with disconnected support. Throughout presenting theoretical and empirical results, we have justified the specific structure of our model. We observe that MMGAN excels in the generative modeling task and successfully clusters the real data in the latent space, regarding the labels in the used datasets. In the conducted experiments, we observed an outstanding performance compared to other two state-of-the-art models which are related to this field.

## References

- [Arjovsky and Bottou 2017] Arjovsky, M., and Bottou, L. 2017. Towards Principled Methods for Training Generative Adversarial Networks. In *5th International Conference on Learning Representations, ICLR 2017, Toulon, France, April 24-26, 2017, Conference Track Proceedings*.
- [Arjovsky, Chintala, and Bottou 2017] Arjovsky, M.; Chintala, S.; and Bottou, L. 2017. Wasserstein Generative Ad-

- versarial Networks. In *International Conference on Machine Learning*, 214–223.
- [Ben-Yosef and Weinshall 2018] Ben-Yosef, M., and Weinshall, D. 2018. Gaussian Mixture Generative Adversarial Networks for Diverse Datasets, and the Unsupervised Clustering of Images. *arXiv*. <http://arxiv.org/abs/1808.10356>.
- [Blum, Hopcroft, and Kannan 2015] Blum, A.; Hopcroft, J.; and Kannan, R. 2015. *Foundations of Data Science*. Cambridge University Press.
- [Chen et al. 2016] Chen, X.; Duan, Y.; Houthoofd, R.; Schulman, J.; Sutskever, I.; and Abbeel, P. 2016. InfoGAN: Interpretable Representation Learning by Information Maximizing Generative Adversarial Nets. *arXiv*. <http://arxiv.org/abs/1606.03657>.
- [Cybenko 1989] Cybenko, G. 1989. Approximation by Superpositions of a Sigmoidal Function. *Mathematics of control, signals and systems* 2(4):303–314.
- [Dilokthanakul et al. 2016] Dilokthanakul, N.; Mediano, P. A. M.; Garnelo, M.; Lee, M. C. H.; Salimbeni, H.; Arulkumaran, K.; and Shanahan, M. 2016. Deep Unsupervised Clustering with Gaussian Mixture Variational Autoencoders. *arXiv*. <http://arxiv.org/abs/1611.02648>.
- [Goodfellow et al. 2014] Goodfellow, I.; Pouget-Abadie, J.; Mirza, M.; Xu, B.; Warde-Farley, D.; Ozair, S.; Courville, A.; and Bengio, Y. 2014. Generative Adversarial Nets. In *Advances in Neural Information Processing Systems*, 2672–2680.
- [Gurumurthy, Sarvadevabhatla, and Babu 2017] Gurumurthy, S.; Sarvadevabhatla, R. K.; and Babu, R. V. 2017. DeLiGAN: Generative Adversarial Networks for Diverse and Limited Data. In *2017 IEEE Conference on Computer Vision and Pattern Recognition, CVPR 2017, Honolulu, HI, USA, July 21-26, 2017*, 4941–4949.
- [Heil 2019] Heil, C. 2019. *Introduction to Real Analysis*. Graduate texts in mathematics. Springer International Publishing.
- [Hopcroft and Kannan 2013] Hopcroft, J., and Kannan, R. 2013. *Foundations of Data Science*. New York: Cornell University.
- [Hornik 1991] Hornik, K. 1991. Approximation Capabilities of Multilayer Feedforward Networks. *Neural Networks* 4(2):251–257.
- [Jolicoeur-Martineau 2018] Jolicoeur-Martineau, A. 2018. The relativistic discriminator: a key element missing from standard GAN. *arXiv*. <http://arxiv.org/abs/1807.00734>.
- [Jost, Jürgen 2008] Jost, Jürgen. 2008. *Riemannian Geometry and Geometric Analysis*, volume 42005. Springer-Verlag, Berlin Heidelberg.
- [Khayatkhoei, Singh, and Elgammal 2018] Khayatkhoei, M.; Singh, M. K.; and Elgammal, A. 2018. Disconnected Manifold Learning for Generative Adversarial Networks. In *Advances in Neural Information Processing Systems 31: Annual Conference on Neural Information Processing Systems 2018, NeurIPS 2018, 3-8 December 2018, Montréal, Canada.*, 7354–7364.
- [Khrulkov and Oseledets 2019] Khrulkov, V., and Oseledets, I. 2019. Universality Theorems for Generative Models. *arXiv*. <http://arxiv.org/abs/1905.11520>.
- [Kingma and Ba 2015] Kingma, D. P., and Ba, J. 2015. Adam: A Method for Stochastic Optimization. In *3rd International Conference on Learning Representations, ICLR 2015, San Diego, CA, USA, May 7-9, 2015, Conference Track Proceedings*.
- [Kingma and Welling 2013] Kingma, D. P., and Welling, M. 2013. Auto-encoding Variational Bayes. *arXiv*. <http://arxiv.org/abs/1312.6114>.
- [LeCun and Cortes 2010] LeCun, Y., and Cortes, C. 2010. MNIST handwritten digit database. <http://yann.lecun.com/exdb/mnist/>.
- [Makhzani et al. 2015] Makhzani, A.; Shlens, J.; Jaitly, N.; and Goodfellow, I. J. 2015. Adversarial Autoencoders. *arXiv*. <http://arxiv.org/abs/1511.05644>.
- [Mukherjee et al. 2018] Mukherjee, S.; Asnani, H.; Lin, E.; and Kannan, S. 2018. ClusterGAN: Latent Space Clustering in Generative Adversarial Networks. *arXiv*. <http://arxiv.org/abs/1809.03627>.
- [Munkres 2017] Munkres, J. 2017. *Topology*. Math Classics. Pearson.
- [Nagarajan and Kolter 2017] Nagarajan, V., and Kolter, J. Z. 2017. Gradient descent GAN optimization is locally stable. In *Advances in Neural Information Processing Systems*, 5585–5595.
- [Nene, Nayar, and Murase 1996] Nene, S. A.; Nayar, S. K.; and Murase, H. 1996. Columbia Object Image Library (COIL-20). Technical report, Columbia University.
- [Pedregosa et al. 2011] Pedregosa, F.; Varoquaux, G.; Gramfort, A.; Michel, V.; Thirion, B.; Grisel, O.; Blondel, M.; Prettenhofer, P.; Weiss, R.; Dubourg, V.; Vanderplas, J.; Passos, A.; Cournapeau, D.; Brucher, M.; Perrot, M.; and Duchesnay, E. 2011. Scikit-learn: Machine Learning in Python. *Journal of Machine Learning Research* 12:2825–2830.
- [Xiao, Rasul, and Vollgraf 2017] Xiao, H.; Rasul, K.; and Vollgraf, R. 2017. Fashion-MNIST: a Novel Image Dataset for Benchmarking Machine Learning Algorithms. *arXiv*. <http://arxiv.org/abs/1708.07747>.